Research Paper

Three-dimensional label-free visualization of the interactions of PM2.5 with macrophages and epithelial cells using optical diffraction tomography

Wang Sik Lee [a],[1], Inha Kang [b],[1], Sung-Jin Yoon [a], Hyunjung Kim [a], Yugyeong Sim [a],[c], Youngjun Park [a], Jinah Park [b],[*], Jinyoung Jeong [a],[c],[**]

[a] Environmental Disease Research Center, Korea Research Institute of Bioscience and Biotechnology (KRIBB), 125 Gwahak-ro, Yuseong-gu Daejeon, 34141, Republic of Korea
[b] School of Computing, Korea Advanced Institute of Science and Technology (KAIST), 291 Daehak-ro, Yuseong-gu Daejeon, 34141, Republic of Korea
[c] Department of Nanobiotechnology, KRIBB School of Biotechnology, University of Science and Technology (UST), 217 Gajeong-ro, Yuseong-gu Daejeon, 34113, Republic of Korea

HIGHLIGHTS

- We visualize the interaction between PM2.5 and cells without labeling agents.
- We demonstrate that ODT enables tracking of intracellular PM2.5 in real-time.
- We propose a method of providing quantitative information on the cellular uptake of PM2.5 over time.
- We show that ODT can visualize the differences in the behavior of macrophages and epithelial cells to PM2.5.

GRAPHICAL ABSTRACT
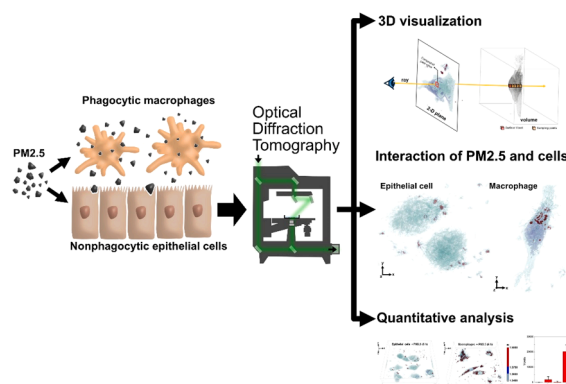
ABSTRACT

Particulate matter ≤ 2.5 µm (PM2.5) poses health risks related to various diseases and infections. However, the interactions between PM2.5 and cells such as uptake and cell responses have not been fully investigated despite advances in bioimaging techniques, because the heterogeneous morphology and composition of PM2.5 make it challenging to employ labeling techniques, such as fluorescence. In this work, we visualized the interaction between PM2.5 and cells using optical diffraction tomography (ODT), which provides quantitative phase images by refractive index distribution. Through ODT analysis, the interactions of PM2.5 with macrophages and epithelial cells, such as intracellular dynamics, uptake, and cellular behavior, were successfully visualized without labeling techniques. ODT analysis clearly shows the behavior of phagocytic macrophages and

* Corresponding author.
** Corresponding author at: Environmental Disease Research Center, Korea Research Institute of Bioscience and Biotechnology (KRIBB), 125 Gwahak-ro, Yuseong-gu Daejeon, 34141, Republic of Korea.
E-mail addresses: jinahpark@kaist.ac.kr (J. Park), jyjeong@kribb.re.kr (J. Jeong).
[1] These authors contributed equally.

nonphagocytic epithelial cells for PM2.5. Moreover, ODT analysis could quantitatively compare the accumulation of PM2.5 inside the cells. PM2.5 uptake by macrophages increased substantially over time, but uptake by epithelial cells increased only marginally. Our findings indicate that ODT analysis is a promising alternative approach to visually and quantitatively understanding the interaction of PM2.5 with cells. Therefore, we expect ODT analysis to be employed to investigate the interactions of materials and cells that are difficult to label.

1. Introduction

Particulate matter (PM) is defined as inhalable particles consisting of a mixture of liquid droplets and solid particles, including black carbon, metals, ammonia, nitrates, sulfates, and water [13,18,27,29,52]. In particular, PM2.5, particles with an aerodynamic diameter less than 2.5 µm, can induce cardiovascular diseases, cancer, asthma, and chronic obstructive pulmonary disease [3,38,48,50]. Numerous toxicological studies of PM2.5 have focused predominantly on toxic effects such as mortality, inflammatory response, and oxidative stress [14,35,49,53]. Understanding the interaction between PM2.5 and cells, including uptake, accumulation, and cell responses, are important to predict the potential risks of PM2.5 [12,23,40]. However, studies on the interactions between PM2.5 and cells are limited. Generally, labeling techniques, such as fluorescence or radioisotopes, were employed to investigate the interaction between particles and cells [45]. However, PM2.5 has a broad size distribution, heterogeneous morphology, and complex compositions, disturbing the employment of labeling agents. Therefore, developing a novel analytical method is necessary to investigate the interaction between PM2.5 and cells.

In several studies, fluorescence-labeled polystyrene (PS) beads were employed to evaluate biodistribution instead of PM2.5 [26,42]. However, morphological and physicochemical characteristics affect the biological fate of particles, such as uptake, biodistribution, clearance, and toxicity [23,30,5]. Since PS beads are homogeneous in size and shape, the interactions of PS beads with biological systems may differ from those of PM2.5. Thus, PM2.5 should be used in studies of their biological fate. Transmission electron microscopy (TEM) has been generally employed to observe PM2.5 absorbed by cells [15,31]. However, TEM provides only two-dimensional (2D) images and requires extreme vacuum, a high-intensity electron beam, and pretreatment for fixation, indicating that TEM is inappropriate for observing the interaction between PM2.5 and cells. Recently, scanning electron-assisted dielectric microscopy (SE-ADM) was introduced to overcome the limitation of TEM analysis for the interaction of PM2.5 and cells [32]. SE-ADM allows nanoscale observation of PM2.5 incorporated into living mammalian cells in aqueous solution without pretreatment for fixation. However, since SE-ADM also provides 2D images, further analysis using confocal Raman microscopy, which includes a fixation process, is required to confirm whether PM2.5 is located inside the cell. To overcome the limitations of analyzing the interaction of PM2.5 with cells, we employed optical diffraction tomography (ODT) for three-dimensional label-free visualization of the interaction between PM2.5 and cells.

ODT is an interferometric technique for capturing three-dimensional (3D) data using the refractive index (RI) distribution of a sample [41]. ODT provides a label-free analysis based on RI, which is an intrinsic optical parameter of materials. This indicates that the ODT can visualize PM2.5 and cells without labeling agents or pretreatment. ODT can visualize intracellular components through 3D reconstruction by measuring the 3D RI. Recently, ODT has been employed for the real time imaging of biological samples, such as red blood cells, hepatocytes, and bacteria [10,20,24]. Moreover, ODT can be used for 3D visualization and quantitative analysis of lipid droplet accumulation, the uptake of gold nanoparticles by cells, and biodegradable polymer production in individual live bacterial cells [19,33,9]. This implies that ODT technology can analyze interactions with live cells in real time. Thus, we employed ODT to investigate the interaction between PM2.5 and cells without labeling techniques.

This study visualized the interaction of PM2.5 with macrophages and epithelial cells using ODT-based holotomography microscopy (HTM). Macrophages engulf exogenous substances such as PM2.5, and epithelial cells are involved in physical barriers and innate immune responses [51]. This indicates that phagocytic macrophages and nonphagocytic epithelial cells will have different interactions with PM2.5. To date, most studies have mainly suggested the toxic effects of the response of cells to PM2.5, such as dose-dependent cytotoxicity or expression of transcription factors. Moreover, bioimaging of cells exposed to PM2.5 has focused on immunofluorescent staining for biomarkers. We used ODT to visualize the interaction of PM2.5 with phagocytic macrophages and nonphagocytic epithelial cells for the first time. Since the PM2.5 and cells were distinguishable by RI distribution, ODT was definitely applicable for visualization. The movement of PM2.5 in the cell was observed by reconstructing the image in 3D based on the RI distribution, and the uptake pattern according to the cell type was also confirmed. Through visualization of the interaction of PM2.5 with macrophages and epithelial cells, we show that ODT can be utilized for intracellular tracking and cellular behavior studies of substances that are difficult to label, such as PM2.5.

2. Experimental section

2.1. Materials

Particulate matter $\leq$ 10 µm (PM10) reference materials (i.e., European reference materials CZ-100) were purchased from Sigma—Aldrich (St. Louis, MO, USA). Ethyl alcohol (anhydrous, 99.9 %) was purchased from SAMCHUN Chemicals (Seoul, Korea).

2.2. Separation of PM2.5

PM2.5-like particles were prepared from PM10 using a modified sedimentation-based separation method [6]. Five hundred milligrams of PM10 was prepared in ethyl alcohol at 1 mg/mL with sonication (DH. WUC. A03H, DAIHAN Scientific, Daegu, KOREA) for 15 min, and the sonication-treated PM10 solution was sedimented for 30 min at room temperature. After 30 min, 50 mL of the supernatant was collected, and the solvent and PM were separated using a centrifuge at 3220g for 5 min (centrifuge 5810, Eppendorf, Hamburg, Germany). After removing the solvent, the pellet was collected in a glass vial using 2 mL of ethyl alcohol and dried in a vacuum oven at 80 °C. By repeating this process ten times, the supernatant and sediments were collected. The PM collected from the supernatant corresponded to PM2.5-like particles, and the precipitate corresponded to PM10-like particles. Moreover, the size distribution of the PM2.5 samples was evaluated by particle analysis using ImageJ software [1,2,37]. First, the PM2.5 image obtained from an optical microscope was converted into a binary image by adjusting the threshold. This method distinguishes the particles from the background. Second, the area of the adjusted image was analyzed using the analytical particle function of ImageJ. In this process, the calculation range was set up at least an area of 1 µm^2 to distinguish it from PM. Finally, the average diameter of the PM2.5 particles was determined using the calculated area values. Since PM2.5 particles have an irregular shape, we calculated the diameter of the sphere and square from the area data and obtained the average value of these values. This method is time-efficient and appropriate for the analysis of numerous particles.

2.3. Compositional analysis of PM2.5

Compositional analysis of the separated PM2.5 was employed to identify elements, water-soluble inorganic ions, and organic compounds. Elemental analysis was performed by scanning electron microscopy-energy-dispersive X-ray spectroscopy (SEM-EDX) and X-ray fluorescence spectrometry (XRF). First, PM2.5 was prepared on a silicon wafer and coated with osmium (HPC—1SW, Vacuum Device Inc., Mito, Japan) for SEM image collection. The SEM images were collected by a field emission SEM instrument (Magellan400, FEI Company, Hillsboro, OR, USA) with an acceleration voltage of 10 kV. Elemental analysis of the samples was performed by mapping analysis using an EDX detector. The separated PM samples were further measured using ICP—MS (Agilent ICP—MS 7700 S, Agilent, Santa Clara, CA, USA). Finally, XRF (PHILIPS PW2404, Amsterdam, Netherlands) was employed to identify the elements in the samples. Water—soluble inorganic ions were analyzed by ion chromatography (IC, 881 Compact IC pro, 844 UV/VIS Compact IC, Metrohm, Herisau, Switzerland) and inductively coupled plasma optical emission spectrometry (ICP-OES, OPTIMA 7300 DV, Perkin-Elmer, Waltham, MA, USA). PM2.5 (200 mg) was extracted in 20 mL distilled water (DW) for three days. The solutions were filtered through 0.45 μm PTFE syringe filters and analyzed using IC and ICP-OES. Anions and ammonium ions (NH_4^+) were measured by IC, and cations excluding NH_4^+ were measured by ICP-OES. The organic compounds in the PM2.5 were analyzed using gas chromatography-mass spectrometry (GC-MS).

The GC-MS system consisted of a gas chromatograph (Agilent Technologies 7890A-GC, Agilent, Santa Clara, CA, USA) and a time-of-flight mass spectrometer (LECO PEGASUS BT-MS, St. Joseph, MI, USA). The samples were added to nine volumes (w/v) of methanol and extracted using an ultra-sonicator (Sonics & Materials Inc., Newtown, CT, USA). The samples were centrifuged at 3000*g* for 5 min, and the supernatants were analyzed using GC-MS.

2.4. 3D morphology analysis of PM2.5

To determine the 3D morphology, ODT images of PM2.5 particles in distilled water (DW) were analyzed using HTM (3D Cell Explorer-fluo, Nanolive, Lausanne, Switzerland). HTM has 200 nm of lateral resolution and 400 nm of axial resolution. Moreover, the illumination source of HTM was based on the Class I laser low power ($\lambda = 520$ nm, sample exposure 0.2 mW/mm^2). The microscope objective used the dry objective lens with 60x magnification, and a numerical aperture was 0.8. The holograms were recorded with an image sensor (CMOS camera, Sony, IMX174, Tokyo, Japan). The ODT analysis consisted of stacked hologram image capturing and volume rendering. First, hologram images of PM2.5 were obtained by HTM, respectively. Then, 3D visualization of the stacked hologram images was performed through the volume rendering process.

2.5. Volume rendering

In this work, we performed volume rendering utilizing the medical imaging interaction toolkit (MITK) [47]. After identifying the volume intensity through the two-dimensional RI map, RGBA control points were set based on the intensity. Visualization was performed by assigning appropriate color and transparency values with the one-dimensional transfer function. The outside of the volume was made relatively transparent by lowering the alpha value, and the inside of the volume was given lower relative transparency by increasing the alpha value, so that both the inside and outside of the volume could be observed from any angle.

2.6. Cell culture

The mouse lung epithelial cell line MLE-12 was cultured in

Dulbecco's medium Ham's F12 (50:50 mix containing L-glutamine) supplemented with 2 % (v/v) fetal bovine serum, antibiotic-antimycotic solution (Gibco, 15240096), ITS liquid media supplement (Sigma, I3146), 10 nM hydrocortisone, 10 nM β-estradiol, and 10 mM HEPES. For the differentiation of bone marrow-derived macrophages (BMDMs), femurs were removed from C57/BL6 mice, and the bone marrow was flushed with RPMI medium. Cells were cultured in RPMI medium containing 25 % (v/v) conditioned medium of L929 cells cultured for 7 days at 37 °C in a 5 % CO_2 atmosphere. BMDM-conditioned medium was replaced every 3 days.
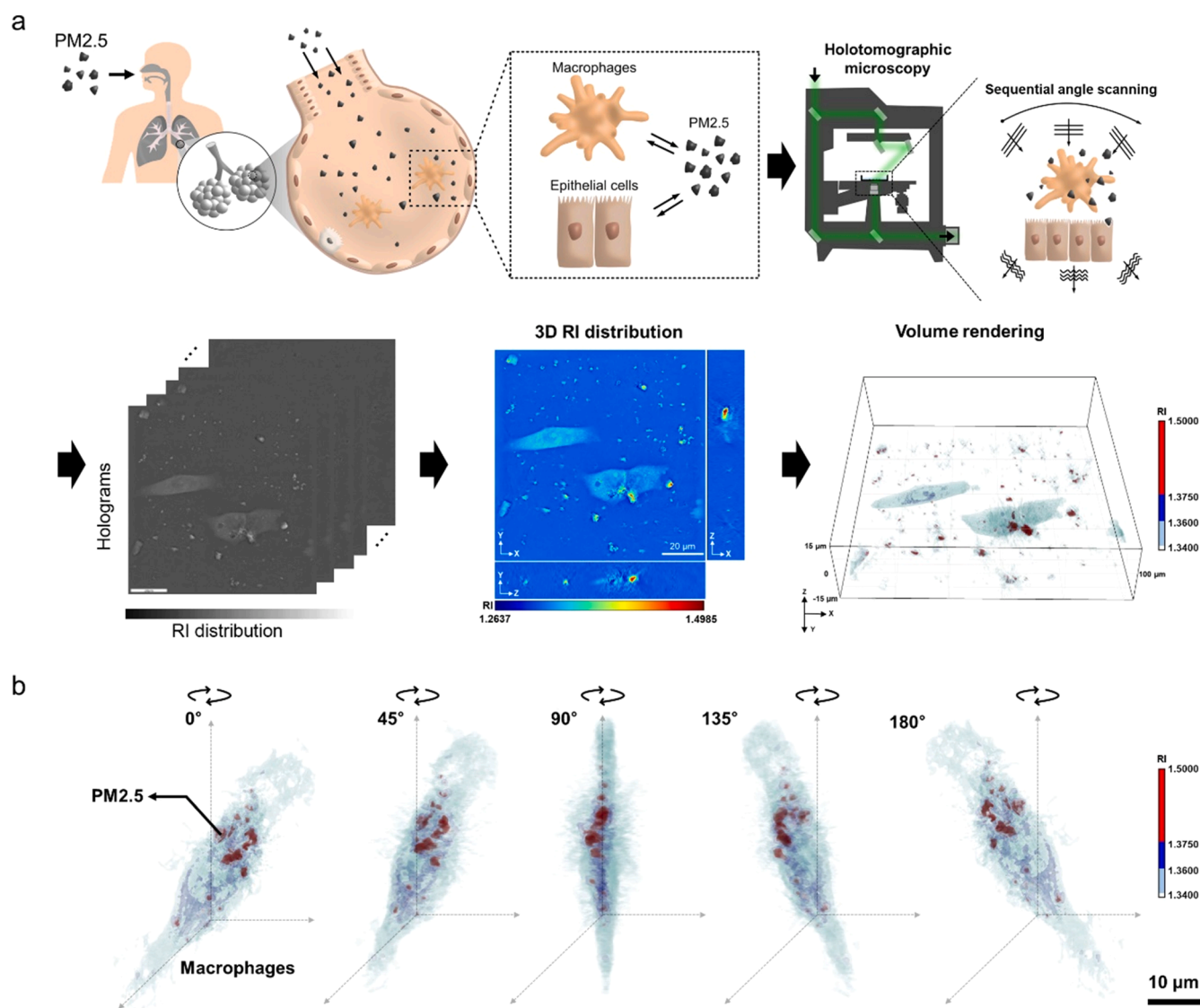
2.7. ODT analysis of the interaction between PM2.5 and cells

BMDMs and MLE-12 cells (1×10^5 cells) were subcultured in tissue culture dishes (FluoroDish) for ODT analysis. We employed a concentration of PM2.5 with a low toxicological effect by referred our previous study [34]. In an analysis of tracking, we required a relatively low concentration of PM2.5 to observe their movement inside the cells without toxicological effects. Thus, we used 10 μg/cm^2 of PM2.5 to evaluate the tracking inside the cells. PM2.5 (10 μg/cm^2) in phosphate-buffered saline (PBS) was added to BMDMs in RPMI medium and MLE-12 in DMEM, and movement of intracellular PM2.5 was measured at 10-minute intervals using HTM. On the other hand, we were required to observe the more active interaction between PM2.5 and cells in analyzing the cell responses. Thus, we increased the PM2.5 concentration to 25 μg/cm^2 and compared the interaction of macrophages and epithelial cells to PM2.5. PM2.5 (25 μg/cm^2) in PBS was added to BMDM and MLE-12, respectively, and ODT images were measured at 1-hour intervals for 3 h. Furthermore, after 6 h, both types of PM2.5-treated cells (n = 30) were measured by HTM, and the number of voxels corresponding to PM2.5 (i.e., RI ≥1.3750) was analyzed by MITK for quantitative comparison.

3. Results and discussion

3.1. Principles of ODT-based visualization of the interaction between PM2.5 and cells

We visualized PM2.5 and two types of cells (i.e., macrophages and epithelial cells) to validate the usefulness of the ODT-based analysis. BMDMs were employed as a model for investigating the function of macrophages, and the MLE-12 cell line was used as a model for epithelial cells. PM2.5 was prepared by separating from PM10 reference material by the sedimentation-based method, and the average diameter was 2.26 ± 1.31 μm (Fig. S1a). This was similar in size distribution and average diameter (2.42 ± 1.54 μm) to PM2.5 collected by a cascade impactor, a traditional method for separating by aerodynamic diameter (Fig. S1b). Thus, we employed PM2.5 as a particle model, MLE-12 cells as an epithelial cells model, and BMDM as a macrophage model to investigate the interaction between PM2.5 and cells. Fig. 1a shows a schematic illustration of ODT-based 3D label-free visualization using PM2.5 and epithelial cells. First, PM2.5-treated cells were prepared in fluoro-dishes and subjected to sequential angle scanning with HTM. The HTM has a 200 nm lateral resolution and 400 nm axial resolution. Thus, HTM can offer a unique solution for live cell imaging and analysis that enables long-term monitoring of cell morphology and organelles. We analyzed the RI distribution of holograms to establish the RI range for 3D visualization and reconstructed it into 3D images using the MITK [46]. The RI value measured by HTM is relative, meaning it is the difference between the RI of the mounting medium and the RI of the object. The 3D-RI distribution showed the RI range from 1.2637 to 1.4985 with color (middle of Fig. 1a); however, this RI range includes all RI values, including PM2.5, cells, and cell medium. In particular, RI values below 1.3400 usually correspond to the background range, including the cell growth medium and opaque region of PM2.5. Thus, in this study, we set up the RI range from 1.3400 to 1.5000 for 3D visualization by volume

Fig. 1. (a) Schematic illustration of the optical diffraction tomography (ODT)-based analysis for PM2.5 and cells. PM2.5 can interact with epithelial cells and macrophages in the alveolar (Left). HTM is employed to visualize the interaction between PM2.5 and cells. A sample in the dish is illuminated by sequential angle scanning. Holograms are recorded at individual angles. Refractive index (RI) distribution is analyzed in 3D planes, including x-y, y-z, and x-z. Based on the RI distribution, a 3D volume-rendered image is obtained using the medical imaging interaction toolkit (MITK) for more detailed visualization. (b) Multi-angle 3D visualization of PM2.5-treated macrophages.

rendering. Volume rendering is a technique of visualizing three-dimensional volume data on a two-dimensional plane. This projection procedure is called Ray Casting, where one ray from each pixel of the image is cast to the volume data (Fig. S2). When the ray hits the surface of the volume, it penetrates through the volume to the end without stopping, so that the volume is sampled by the ray and is shaded according to the illumination model. After all sampling points are shaded, they are composited along the ray to produce a final color (RGB value) of the pixel currently being processed. The voxels in the volume data are classified according to its property – in our case RI value. The classification is done by applying a transfer function, which maps the range of RI values with RGB and Alpha (opacity) values. It indicates that ODT can visualize particles and cells separately through the color assignment and opacity adjustment. For example, we can make the RI values associated with the cell semitransparent, while the RI values of the particles opaque. In this way, we can observe the particles within the cell (See Fig. S6). Therefore, we were able to investigate interactions between PM2.5 and cells, such as uptake and cellular response, using 3D

visualization by volume rendering.

In the analysis of ODT, we could obtain the 3D image for PM2.5 and cells, indicating that ODT enables stereoscopic characterization through various angle adjustments. The 3D volume-rendered images (Movies S1–S3) show approximately realistic morphologies of the PM2.5, macrophage, and PM2.5-treated macrophage in various angles. Particularly, Fig. 1b shows multi-angle 3D images of live macrophages after 1 h of PM2.5 exposure, which was obtained by volume rendering with color stating and opacity adjustment. This multi-angle analysis indicates that the ODT analysis can discriminate whether the location of PM2.5 was extracellular or intracellular. In Fig. 1b, the red color with a relatively high RI range indicated PM2.5 and the 3D image with an angle of 90° shows that PM2.5 was located inside the macrophage. This intracellular PM2.5 can be interpreted as a result of the phagocytic behavior of the macrophages, implying that simultaneously PM2.5 can directly affect macrophages. In general, studies on particle-cell interactions can contribute to the progress of the biomedical fields by increasing the understanding of the fate of particles and toxicological mechanisms [12,

4]. It implies that the 3D visualization can give informative evidence to interpret the particle-cell interaction. Kallepitis et al., also suggested the importance of 3D imaging for understanding cell-materials interaction using a confocal Raman spectroscopy [17]. Therefore, in this study, we employed ODT as an analytical tool for 3D visualization of the interaction between PM2.5 and cells and compared differences in response to PM2.5 of macrophages and epithelial cells through 3D visualization by volume rendering.

Supplementary material related to this article can be found online at doi:10.1016/j.jhazmat.2023.131678.

Supplementary material related to this article can be found online at doi:10.1016/j.jhazmat.2023.131678.

Supplementary material related to this article can be found online at doi:10.1016/j.jhazmat.2023.131678.

3.2. Evaluation of morphological characteristics of PM2.5 using ODT

Morphological characterization of PM2.5, including shape and RI distribution, is important in the 3D visualization of the interaction between PM2.5 and cells using ODT. These morphological characteristics could be employed as criteria to distinguish PM2.5 and cells in the 3D visualization. To analyze the morphological characteristics, we measured PM2.5 using HTM and analyzed the RI distribution by MITK. HTM is based on a Mach—Zehnder interferometer that provides quantitative phase images from multiple holograms with various illumination angles. It allows the measurement of the 3D RI distribution of objects, such as living cells and tissues, resulting in 3D visualization. In this study, we first employed HTM to evaluate the complex 3D morphology and RI distribution of PM2.5. PM2.5 was prepared in DW to obtain a 3D holotomographic image. Fig. 2a shows the 3D holotomographic image of PM2.5 measured by HTM and digitally rendered by STEVE software. The color code corresponds to the average value of RI, the morphology of PM2.5 was irregular, and various RI values were shown. To obtain a more detailed 3D morphology, the RI distribution was analyzed using MITK and reconstructed as a 3D image of PM2.5 (Fig. 2b). Moreover, Fig. 2c shows that the 3D morphology of PM2.5 measured by HTM can be visualized from various angles. It indicates that we can visually implement the morphology of PM2.5 closer to the actual shape using HTM. Generally, PM2.5 morphology can be evaluated using SEM or atomic force microscopy (AFM) [39]. However, because the electron beam and probe have limitations in analyzing the interior of the sample, SEM and AFM could only determine the exterior shape of the PM2.5. In contrast, HTM allows 3D morphology analysis of PM2.5 because HTM employed RI as an imaging contrast, indicating that the HTM can also be used as a 3D morphological characterization tool. Fig. 2d shows 3D images and RI distributions of various PM2.5 particles. RI distribution was analyzed from 1.3400, considering the RI of the background (i.e., RI of mounting medium). Most RI distributions of PM2.5 were observed in the range over 1.3750 and differed in each PM2.5, respectively. It implies that each PM2.5 had a heterogenous morphology and composition. To validate this heterogeneity, we analyzed the compositions of PM2.5. As a result of composition analysis, PM2.5 was composed of composite materials, including inorganic elements such as O, Si, Ca, Al, S, K, Mg, Na, Fe, Cl, N, Cu, and Zn, most of the elements were present as compounds such as oxides and sulfides (Fig. S3). Moreover, GC-MS analysis showed that PM2.5 also contained various organic compounds such as polycyclic aromatic hydrocarbons (PAH), UV stabilizers, and plastic additives (Data was not shown). In the quantitative analysis, we validated that PM2.5 was composed of inorganic elements over 90 % (mass balance) and contained about 6 % water-soluble ions (Fig. S4). These suggested that PM2.5 was composed of complex components, indicating that the RI distribution could differ for each PM2.5 particle. PM2.5 compositions can depend on the region or seasons and affect morphological characteristics or RI distribution [16]. Therefore, understanding the accurate characterization of PM2.5 is essential for employing ODT analysis. Based on the characterization of PM2.5, we referred to the

morphological characteristics (i.e., irregular shape and RI distribution) as criteria to discriminate the PM2.5 and cells in the 3D visualization by volume rendering.

3.3. Three-dimensional label-free visualization of PM2.5 and cells using the difference in refractive index

Determination of the RI range in ODT is important for visualizing the interaction between PM2.5 and cells. We compared the differences in RI distribution from the volume data of the PM2.5, cells, and PM2.5-treated cells, respectively (n = 9). Figs. 3a and 3b show the relative frequency of RI values of the PM2.5, the cells (i.e., epithelial cells and macrophages), and PM2.5-treated cells, respectively. While both epithelial cells and macrophages were observed in the RI range lower than 1.3750, RI values of PM2.5 and PM2.5-treated cells were observed higher than 1.3750. Therefore, we distinguished and visualized cells and PM2.5 based on 1.3750. Kim et al. also visualized the accumulation of gold nanoparticles in living cells using ODT, and they distinguished between gold nanoparticles and cells based on the RI value of 1.3750 [19]. Fig. 3c shows a 3D image of MLE-12 cells, which were lung epithelial cells, and the morphology of epithelial cells could be visualized in the RI range of 1.3400–1.3750. Fig. 3d shows images of epithelial cells 6 h after PM2.5 treatment. In Fig. 3d, PM2.5 particles were observed around the epithelial cells, and their RI range was generally higher than 1.3750. Figs. 3e and 3f show 3D images of macrophages and PM2.5-treated macrophages. As with epithelial cells, macrophages could be visualized at RI values under 1.3750, whereas a relatively higher range of (≥1.3750) RI was observed in PM2.5-treated macrophages. RI distribution of PM2.5 was broader than cells, and particularly relatively higher RI values (≥ 1.3750) were measured. It could be attributed to the complex composition of PM2.5, including inorganic elements, ions, and organic compounds (Figs. S2 and S3). These substances generally have higher RI values than cells and organelles (e.g., nucleus and cytoplasm) (Table S1). It implies that the PM2.5 and cells could be separately visualized based on designating a specific RI range.

Interestingly, Fig. 3f shows that PM2.5 was mainly internalized by macrophages through phagocytic behavior. One advantage of ODT-based visualization is that a method to visualize PM2.5 distributed inside the cell using the transfer function. The transfer function converts the RI values of voxels into color and transparency according to characteristics such as intensity or gradient, which can be effectively visualized for PM2.5 inside the cells. Fig. S5 shows the transfer function used for our visualization, and Fig. S6 shows the visualization process using the transfer function. Fig. S6a is the result of rendering only the range of 1.3400–1.3750, which corresponded only to the RI region of the cell and showed only the appearance of the cell. Fig. S6b attempted to analyze PM2.5 by assigning a color to the range of 1.3750 or higher, but only PM2.5 existing outside the cell could be identified. Fig. S6c is an image where the RI distribution was specifically divided and the transparency adjusted, indicating that the ODT analysis with the transfer function can effectively visualize intracellular PM2.5. Thus, Fig. 3d presents that many PM2.5 particles were located inside the macrophages along the nucleus boundary (red dash box in Fig. 3f). It could be interpreted that PM2.5 was located in the phagosome through the phagocytic behavior of macrophages [8]. Therefore, this study shows that the interaction between PM2.5 and cells can effectively be visualized by ODT analysis.

3.4. Label-free tracking of intracellular PM2.5 using ODT

To date, we evaluated the morphological characteristics of PM2.5 and cells to establish the RI range for 3D visualization. Using an optimized RI range, we could visualize the movement of intracellular PM2.5. The HTM can use a chamber capable of maintaining cell growth conditions, including temperature, oxygen concentration, and carbon dioxide concentration, enabling the observation of living cells in real time. Thus, ODT analysis allows real time visualization of the interaction
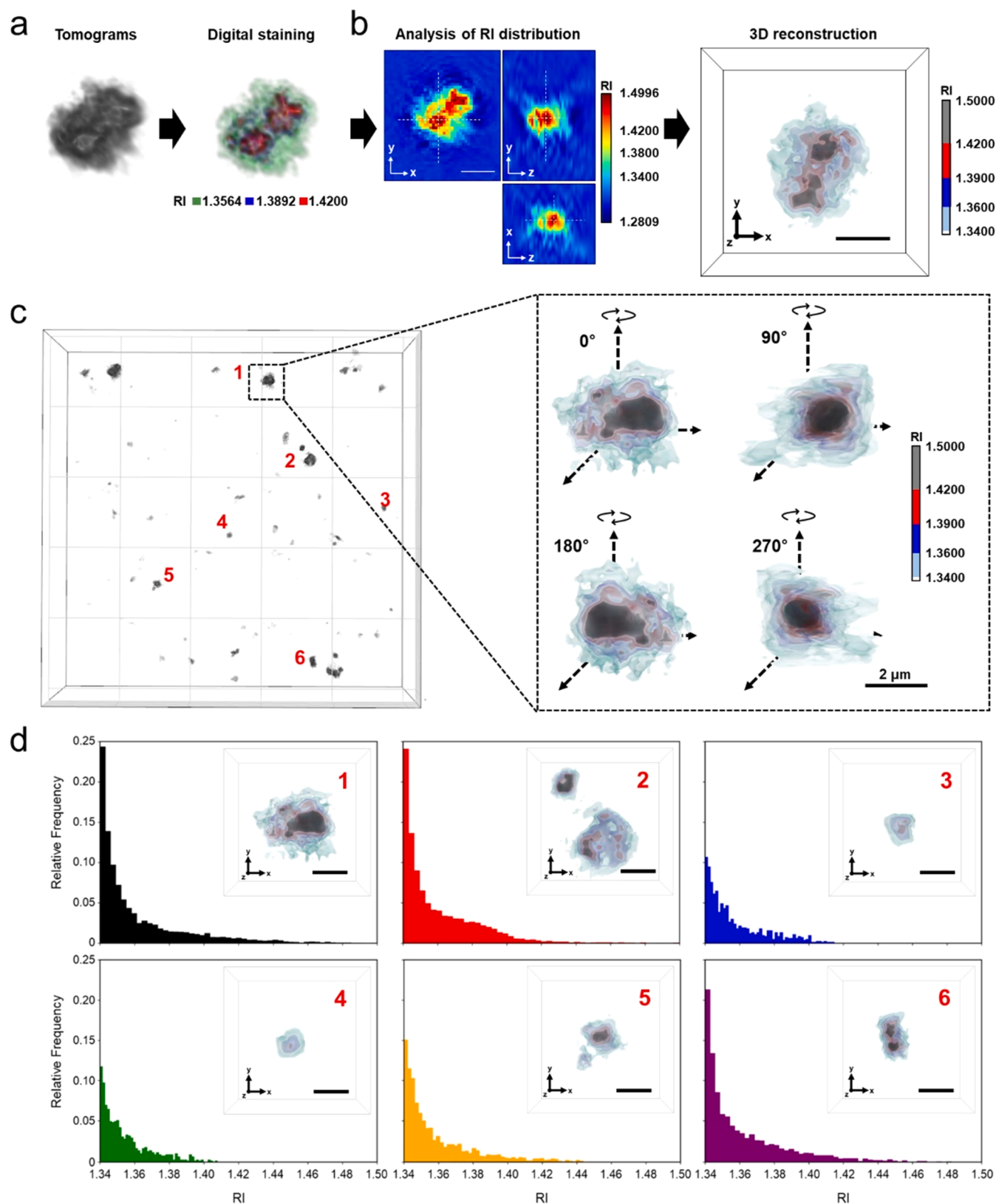
Fig. 2. 3D-Visualization of PM2.5 using HTM. (a) schematic process of ODT for PM2.5 visualization using HTM and STEVE software (Left). Tomogram of PM2.5 has analyzed the RI distribution and 3D-reconstructed by MITK. (b) 3D RI distribution (Left) and 3D volume-rendered image of PM2.5 using MITK (Right, Scale bar: 2 μm). (c) 3D tomogram of PM2.5 and 3D-rendered image by MITK with multiple angles. (d) Various 3D-rendered images of PM2.5 (inset images) and relative frequencies of the number of voxels in each PM2.5 corresponding to a number (Scale bar: 2 μm).
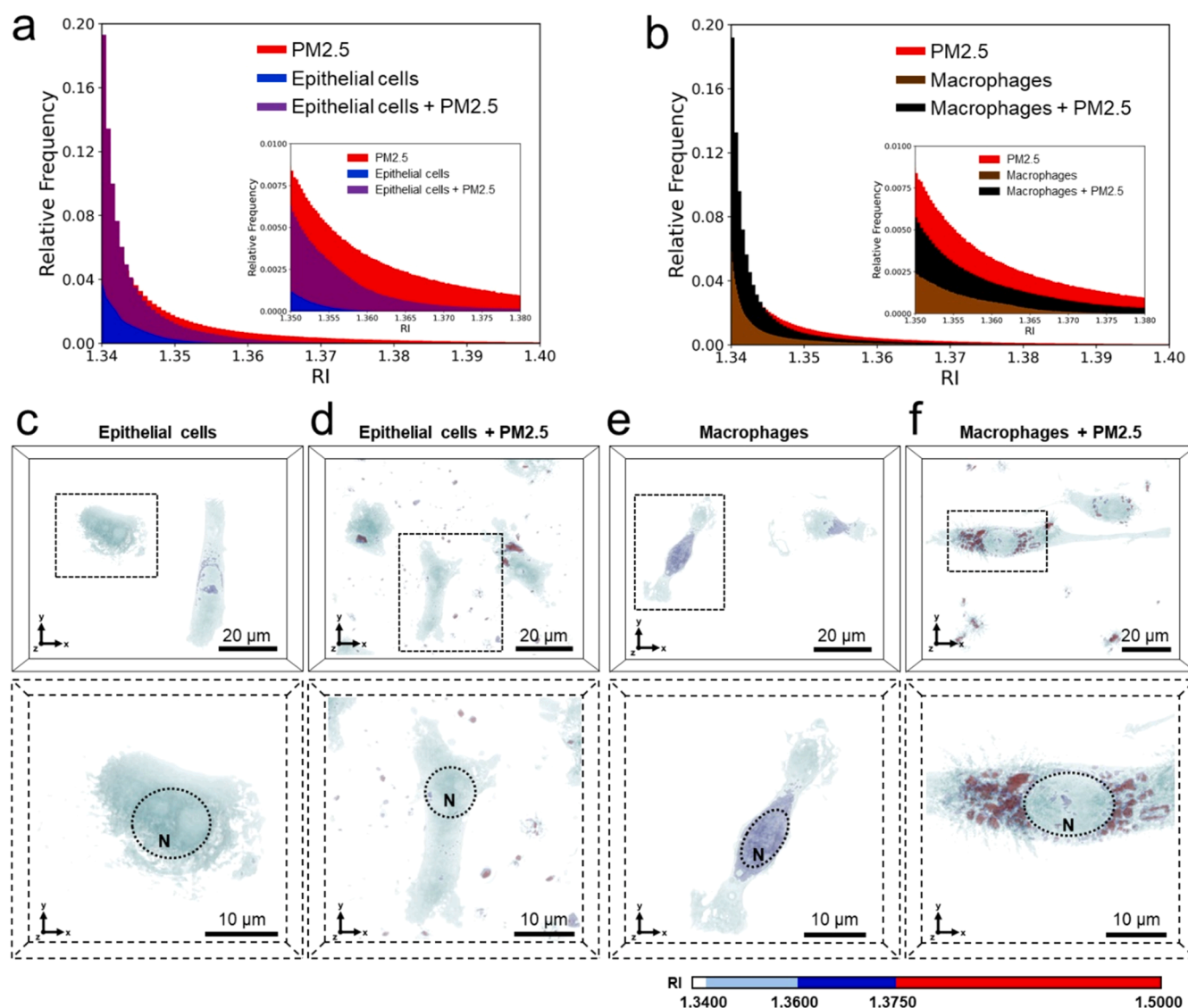
Fig. 3. A distinction between cells and PM2.5 in tomographic images. Relative frequencies of refractive index (RI) distribution of PM2.5, epithelial cells, and macrophages. Comparison of RI distribution; (a) PM2.5, epithelial cells, and PM2.5 treated epithelial cells; (b) PM2.5, macrophages, and PM2.5 treated macrophages. RI distributions are results from averages for nine tomograms (n = 9). 3-D volume-rendered images of epithelial cells (c), PM2.5 treated epithelial cells (d), macrophages (e), and PM2.5 treated macrophages (f). Dash boxes below were magnified images of insert dash boxes in (a ~ d), respectively. The label "N" corresponds to the nucleus, and dotted circles indicate the nucleus of the cells.

between PM2.5 and cells, resulting in label-free tracking, and we could demonstrate the intracellular dynamics of PM2.5 using ODT analysis. The heterogeneous size and composition of PM2.5 made it challenging to apply the labeling technology, resulting in limitations for evaluating uptake and tracking within cells. Thus, we employed the ODT analysis to investigate the uptake and intracellular tracking of PM2.5. The heterogeneous size and composition of PM2.5 made it challenging to apply the labeling technology, resulting in limitations for evaluating uptake and tracking within cells. Thus, we employed the ODT analysis to investigate the uptake and intracellular tracking of PM2.5. We observed epithelial cells in real time at 10-minute intervals after PM2.5 treatment (Fig. 4a). The movement of PM2.5 (red arrow, RI ≥1.3750) inside the epithelial cells was visualized over time. Moreover, the front view images in Fig. 4a demonstrate that PM2.5 was located in the cytoplasm of the epithelial cells. This indicates that ODT analysis is suitable for tracking PM2.5 inside live cells without labeling techniques. Fig. 4b shows that PM2.5 was located in the cytoplasm of the macrophages, and a relatively more enormous amount of PM2.5 was observed inside the macrophages over time (red arrows in Fig. 4b) than in epithelial cells due to their

phagocytic behavior. In particular, the process of PM2.5 uptake on the surface of macrophages was observed at 20 min and 30 min after PM2.5 treatment (blue arrows and dotted boxes in Fig. 4b). It was similar to phagosome formation and showed that macrophages actively interact with PM2.5 [43,44]. Generally, there were some techniques for 3D morphological characterization, such as atomic force microscopy or X-ray-based synchrotron radiation [11,39]. Although these techniques can provide the 3D morphology and compositional information of PM2.5, they have limitations in evaluating the interaction of PM with cells in the real time and native state. In this study, we demonstrated that ODT could provide the 3D morphological characteristics of PM2.5 and information on their interactions with cells, including uptake and cell response. Moreover, Fig. 4 shows not only that intracellular marker-free tracking is possible using ODT but also the difference in cell responses between epithelial cells and macrophages in terms of interaction with PM2.5. Thus, we further analyzed differences in response to PM2.5 by cell types using ODT.
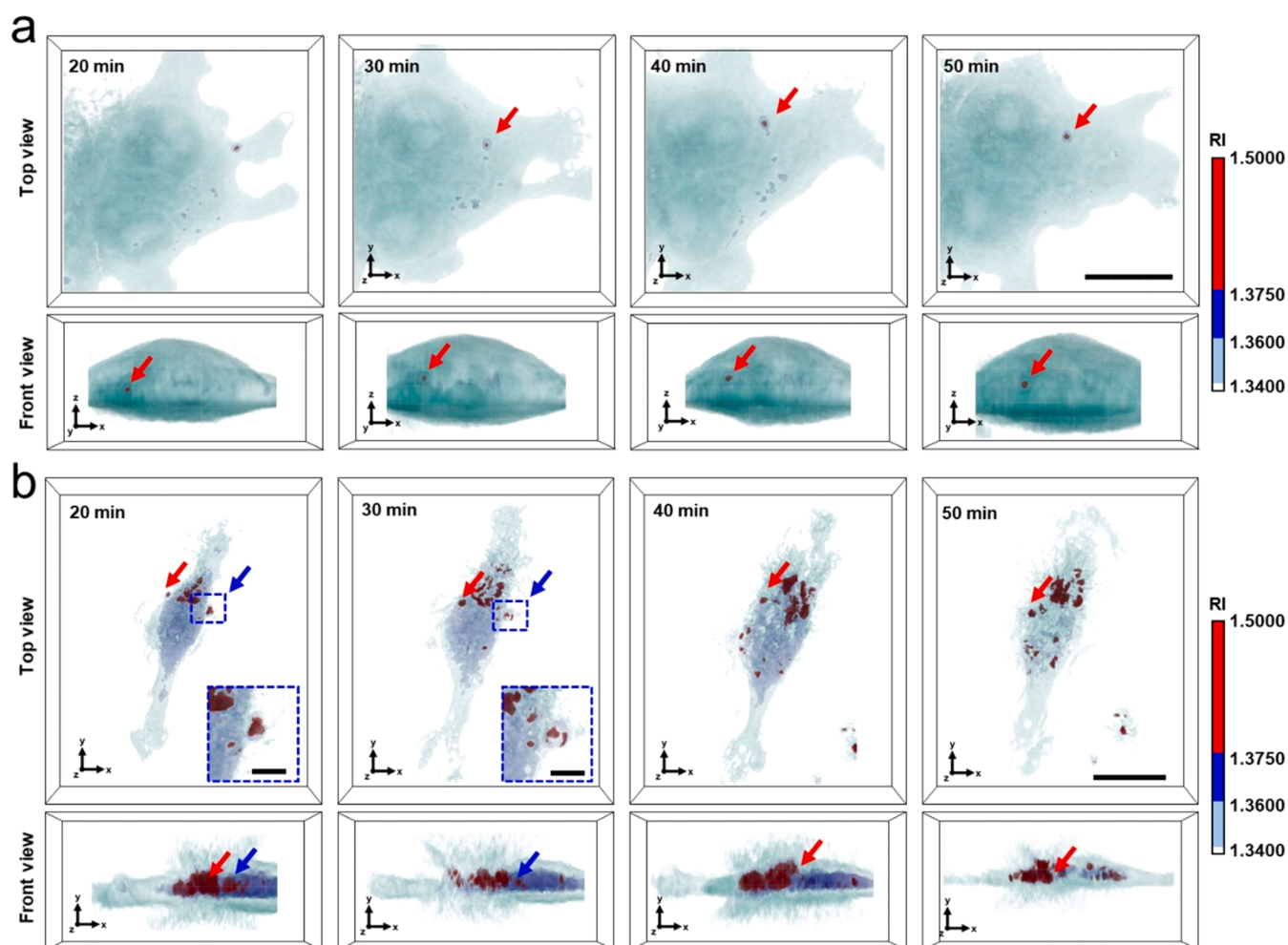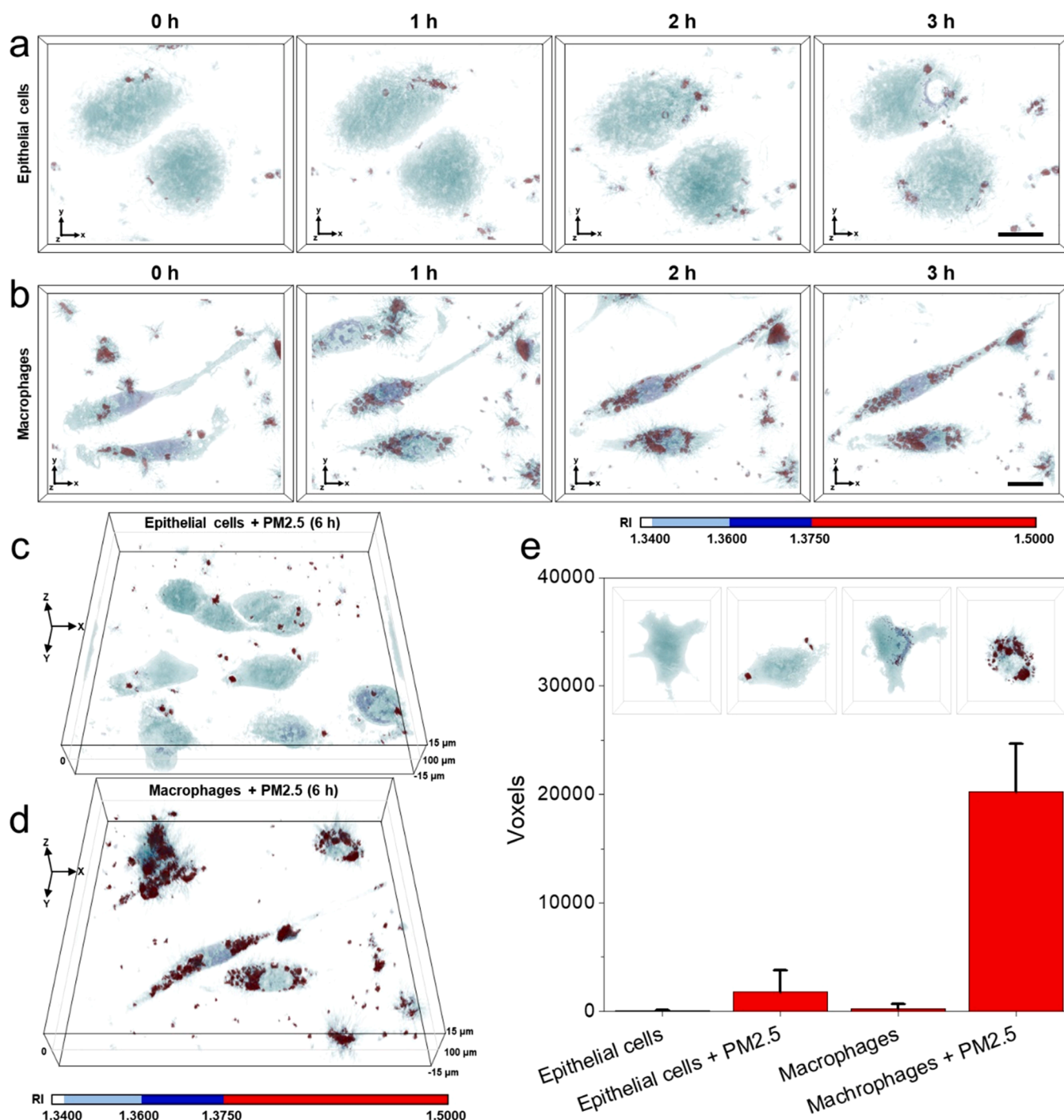
Fig. 4. Label-free tracking of PM2.5 in epithelial cells and macrophages. 3D volume-rendered images of PM2.5-treated epithelial cells (a) and macrophage (b) were observed at 10-minute intervals (Scale bar: 10 μm). In PM2.5-treated macrophage (b), the procedure of PM2.5 uptake by macrophage was observed (inset images at 20 and 30 min, blue arrows, scale bar: 2 μm). The upper images indicate the top view, and the below images indicate the front view of 3-D volume-rendered images. All red arrows indicate PM2.5.

3.5. Visualization of the difference in uptake patterns of PM2.5 by macrophages and epithelial cells

ODT analysis provides visualization of the 3D morphological characterization of PM2.5 and its interactions with cells in real time. In addition, ODT analysis enables quantitative analysis using voxels, which represent regular lattice units in 3D space. We compared the phagocytic behavior of macrophages and the nonphagocytic behavior of epithelial cells toward PM2.5 using ODT analysis in terms of visualization and quantification. To investigate the interaction between PM2.5 and the two types of cells, we observed the PM2.5-treated epithelial cells and macrophages in real time at 1-hour intervals for three hours. In Fig. 5a, PM2.5 was mainly observed in the outer part of the epithelial cells. Moreover, we counted the number of voxels of PM2.5 in epithelial cells over time for quantitative analysis. In this study, the voxel number indicates the total sum of RI values corresponding to intracellular PM2.5 (≥1.3750). The voxel numbers corresponding to the RI of PM2.5 in epithelial cells (≥1.3750) were 724, 1898, 1808, and 1674 over time, indicating that PM2.5 uptake by epithelial cells was not time-dependent. It could be interpreted as the feature of epithelial cells acting as a physical barrier to protect the translocating of PM2.5 to other organs [51]. On the other hand, Fig. 5b shows that PM2.5 uptake into macrophages increased over time. This shows that the interaction of macrophages with PM2.5, an exogenous substance, differs from that of

epithelial cells. Macrophages play an essential role in recognizing and processing PM2.5, reducing risks from exposure to PM2.5 [25]. It implies that the macrophages actively interact with PM2.5, including phagocytosis. Therefore, we focused more on the interaction between PM2.5 and macrophages. We furtherly observed how macrophages responded to PM2.5 exposure (Fig. S7). The macrophages changed shape or migrated for more PM2.5 uptake over time (colored boxes and arrows in Fig. S7). Moreover, we observed that the area around the macrophages after 3 h of PM2.5 treatment was clean than after 1 h (Fig. S7), indicating the phagocytic behavior of the macrophages. It was visually validated in the single macrophage level (Fig. S8a) and compared the number of voxels over time (Fig. S8b). The voxel count corresponding to RI of PM2.5 (≥1.3750) inside macrophages was increased to levels of 3790, 6267, 9239, and 11,965 over time (Fig. S8b). To further observe the uptake of PM2.5, we additionally observed epithelial cells and macrophages until 6 h after PM2.5 treatment. In epithelial cells, PM2.5 was mainly observed in the cell periphery even after 6 h (Fig. 5c). On the other hand, for macrophages, most PM2.5 was located inside the cell (Fig. 5d). To quantitatively compare the two cell types, we analyzed the number of voxels corresponding to RI values of 1.3750 or more for PM2.5-treated epithelial cells and macrophages, respectively (n = 30). Fig. 5e shows that the voxel number of RI corresponding to PM2.5 (≥ 1.3750) was 11-fold higher in macrophages than in epithelial cells, and the insert images in Fig. 5e visually exhibit the

Fig. 5. Difference of PM2.5 uptake by epithelial cells and macrophages. Uptake of PM2.5 in epithelial cells and macrophages by time. 3D volume rendered-images of PM2.5 treated epithelial cells (a) and macrophages (b) for 3 h (Scale bar: 10 μm). 3D volume rendered-images of PM2.5 treated epithelial cells (c) and macrophages (d) after 6 h. (e) Quantitative analysis of PM2.5 in epithelial cells and macrophages (n = 30). Voxels of PM2.5 corresponded over 1.375 of RI from 3-D volume-rendered images, respectively.

voxel number difference between both cell types. It implies that the RI could be used as imaging contrast for 3D visualization and data for quantitative comparison in ODT analysis; moreover, it suggests that the ODT can provide visual and quantitative information for understanding the cell responses to the PM2.5, such as non-phagocytic and phagocytic behaviors. In general, the cellular uptake of PM2.5 was analyzed by TEM. A recent study reported the uptake of biochar fine particles by phagocytic macrophages and non-phagocytic epithelial cells using TEM [28]. The biochar fine particles were observed inside cells, but TEM analysis could only provide 2D images with cells in a non-native state.

However, our study distinctively shows the phagocytic behavior of macrophages and the non-phagocytic behavior of epithelial cells for PM2.5 in real time, and these differences were additionally supported through the voxel analysis (Fig. 5). Consequently, we demonstrated that the macrophages actively interact with PM2.5 by phagocytic behavior, suggesting that PM2.5 exposure may be more likely to induce macrophage damage.

We additionally analyzed the morphological alterations of cells by PM2.5 using ODT. A recent study suggested that PM2.5 impaired macrophage functions, exacerbating pneumococcus-induced pulmonary

pathogenesis, and indirectly provided evidence of macrophage impairment by PM2.5 using fluorescent-labeled latex beads [7]. The ODT analysis could directly demonstrate the impact of PM2.5 on the morphological alteration of cells. Fig. S9 shows the morphological changes of PM2.5-treated epithelial cells and macrophages. Fig. S9a shows the apoptosis-like behavior of epithelial cells after PM2.5 treatment. The cell morphology was changed over time from a long rod shape to a spherical shape. The RI distribution was also increased from 1.3500 to 1.4000. This increase in the RI range could result from apoptosis processes such as cell shrinkage and chromatin condensation. This RI value increase might be misunderstood with a range of PM2.5 RI. Thus, the morphological characteristics (i.e., shape and RI range) should be considered when analyzing the results from 3D visualization. Fig. S9b shows the cell division process of PM2.5-treated epithelial cells, which indicates that PM2.5 exposure had a non-significant effect on cell growth. Fig S9c shows that the PM2.5-treated macrophages were shortened in cell lengths from 73.2 μm at 14 h to 36.2 μm at 20 h, and membrane blebbing (red arrow in Fig S9) was formed. We evaluated macrophage without PM2.5 treatment, and it showed the morphological changes of hydrogen peroxide (100 μM)-treated macrophage. The length of the macrophage was decreased from 81.2 μm to 46.9 μm, and membrane blebbing, a feature of apoptosis, was also observed (Fig. S10). Therefore, Fig. S9c could be interpreted as an apoptotic cell death process. These results indicate that ODT analysis can be used for visualizing the toxicological effects of PM2.5.

This study demonstrated that ODT could evaluate the interaction between PM2.5 and cells, including 3D morphology analysis, uptake, intracellular dynamics, and quantitative analysis (Fig. 6). In recent studies, ODT analysis was mainly employed for the quantitative and visual analysis of intracellular lipid droplet accumulation to overcome the limitations of fluorescence labeling of lipid droplets, including photobleaching and phototoxicity [22,33]. Another study reported the label-free visualization and quantification of polyhydroxyalkanoates in individual bacterial cells using ODT [9]. Moreover, some studies reported a method for intracellular particle analysis using ODT. Kim et al. visualized the appearance of silica particles in macrophages using ODT [21]. This implies that by using ODT as an optical tweezer, it is possible to monitor the responses of cells in real time. Additionally, the charge-dependent uptake of PS nanoparticles and their effects on the morphology of alveolar cells were also analyzed using ODT [36]. These studies show that the application of ODT analysis is expanding. Therefore, we expect that the ODT will be gradually employed more for analyzing particle-cell interactions.

4. Conclusion

This study demonstrated that ODT is a RI-based 3D visualization technique that can analyze the interaction of PM2.5 with cells without labeling techniques in real time. Macrophages and epithelial cells, representative cells that can interact with PM2.5, were used, and PM2.5 uptake and cell responses were visually and quantitatively analyzed by distinguishing the PM2.5 and cells based on RI distribution. We visualized the phagocytic behavior of macrophages and the nonphagocytic behavior of epithelial cells toward PM2.5 through ODT. This showed that interaction with PM2.5 can vary depending on the function of the cell. We also demonstrated that the intracellular dynamics of PM2.5 can be analyzed through real time analysis. In summary, this study highlights the utility of ODT in enabling the real time visualization and quantitative analysis of PM2.5 interactions with individual living cells. Visualization using ODT will be helpful not only for studying PM2.5 of heterogeneous size, shape, and composition but also for studying the intracellular accumulation and dynamics of other environmentally relevant particles for which labeling techniques remain limited.
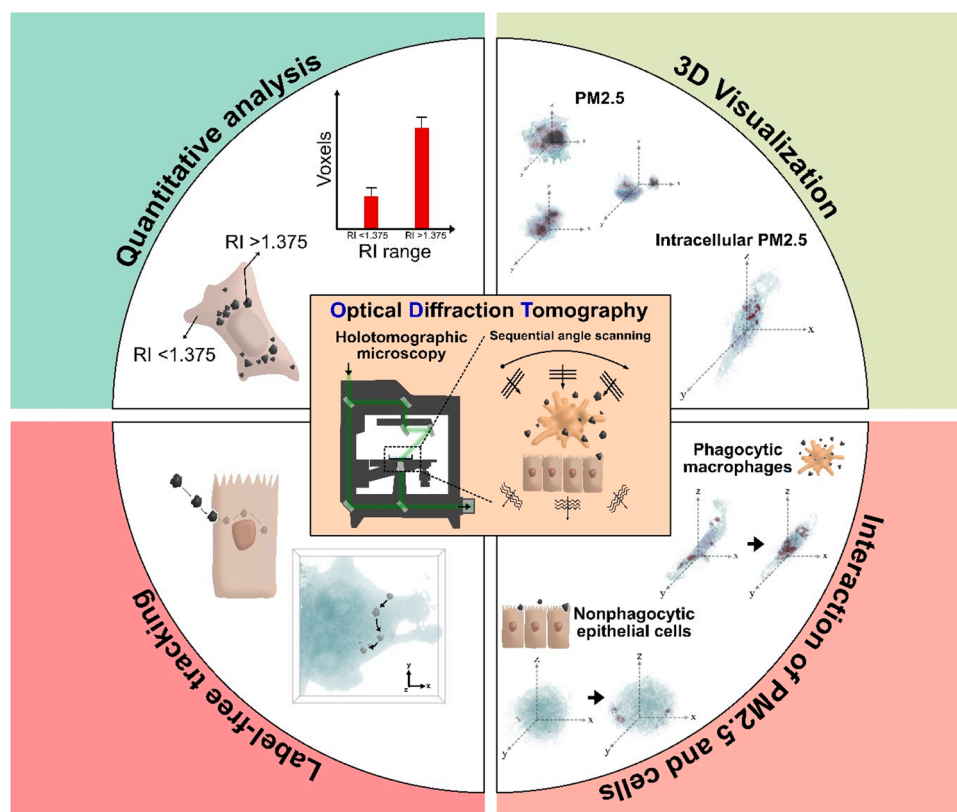
Fig. 6. Schematic illustration of overall features of optical diffraction tomography (ODT) for investigating the interaction between PM2.5 and cells. ODT analysis provides 3D visualization of PM2.5 and cell morphology, differences in the cell responses to PM2.5, and label-free tracking of intracellular PM2.5. Additionally, ODT analysis allows quantitative analysis based on voxel counting.

Environmental implication

PM2.5 exposure can induce various diseases, suggesting that understanding the interaction of PM2.5 with cells is essential to predict potential risks. However, the complex composition and morphology of PM2.5 restrict the application of labeling techniques, disturbing the investigation of PM2.5′s fate and bioaccumulation. This study demonstrated different behaviors of macrophages and epithelial cells toward PM2.5 using optical diffraction tomography (ODT). ODT enables 3D visualization for the tracking, quantitative analysis, and evaluation of the biodistribution of intracellular PM2.5. Our results indicate that ODT can be employed to investigate the intracellular behavior of environmentally relevant materials that are challenging to label.

CRediT authorship contribution statement

Wang Sik Lee: Conceptualization, Methodology, Characterization, Writing – original draft. **Inha Kang:** Visualization, Methodology, Characterization, Writing – review & editing. **Sung-Jin Yoon:** Cell culture, Characterization, Writing – review & editing. **Hyunjung Kim:** Characterization, Writing – review & editing. **Yugyeong Sim:** Characterization, Writing – review & editing. **Youngjun Park**: Funding acquisition, Resources, Project administration, Writing – review & editing. **Jinah Park:** Conceptualization, Visualization, Supervision, Writing – original draft, Writing – review & editing. **Jinyoung Jeong:** Conceptualization, Supervision, Characterization, Writing – original draft, Writing – review & editing. All authors have read and agreed to the published version of the manuscript.

Declaration of Competing Interest

The authors declare that they have no known competing financial interests or personal relationships that could have appeared to influence the work reported in this paper.

Data availability

Data will be made available on request.

Appendix A. Supporting information

Supplementary data associated with this article can be found in the online version at doi:10.1016/j.jhazmat.2023.131678.

References

[1] Abràmoff, M.D., Magalhães, P.J., Ram, S.J., 2004. Image processing with imageJ. Biophotonics Int 11, 36–41. https://doi.org/10.1201/9781420005615.ax4.
[2] Agra, A.A., Nicolodi, A., Flores, B.D., Flores, I.V., da Silva, G.L.R., Vilela, A.C.F., et al., 2021. Automated procedure for coke microstructural characterization in imagej software aiming industrial application. Fuel 304, 121374. https://doi.org/10.1016/j.fuel.2021.121374.
[3] Al-Kindi, S.G., Brook, R.D., Biswal, S., Rajagopalan, S., 2020. Environmental determinants of cardiovascular disease: lessons learned from air pollution. Nat Rev Cardiol 17, 656–672. https://doi.org/10.1038/s41569-020-0371-2.
[4] Borkowska, M., Siek, M., Kolygina, D.V., Sobolev, Y.I., Lach, S., Kumar, S., et al., 2020. Targeted crystallization of mixed-charge nanoparticles in lysosomes induces selective death of cancer cells. Nat Nanotechnol 15, 331–341. https://doi.org/10.1038/s41565-020-0643-3.
[5] Braakhuis, H.M., Park, M.V.D.Z., Gosens, I., De Jong, W.H., Cassee, F.R., 2014. Physicochemical characteristics of nanomaterials that affect pulmonary inflammation. Part Fibre Toxicol 11, 1–25. https://doi.org/10.1186/1743-8977-11-18.
[6] Charoud-Got, J., Emma, G., Seghers, J., Tumba-Tshilumba, M.F., Santoro, A., Held, A., et al., 2017. Preparation of a PM2.5-like reference material in sufficient quantities for accurate monitoring of anions and cations in fine atmospheric dust. Anal Bioanal Chem 409 (7121–7131). https://doi.org/10.1007/s00216-017-0670-6.
[7] Chen, Y.-W., Huang, M.-Z., Chen, C.-L., Kuo, C.-Y., Yang, C.-Y., Chiang-Ni, C., et al., 2020. PM2.5 impairs macrophage functions to exacerbate pneumococcus-induced pulmonary pathogenesis. Part Fibre Toxicol 17, 37. https://doi.org/10.1186/s12989-020-00362-2.
[8] Cheng, W., Kim, S., Zivkovic, S., Chung, H., Ren, Y., Guan, J., 2022. Specific labelling of phagosome-derived vesicles in macrophages with a membrane dye delivered with microfabricated microparticles. Acta Biomater 141, 344–353. https://doi.org/10.1016/j.actbio.2022.01.028.
[9] Choi, S.Y., Oh, J., Jung, J.H., Park, Y.K., Lee, S.Y., 2021. Three-dimensional label-free visualization and quantification of polyhydroxyalkanoates in individual bacterial cell in its native state. Proc Natl Acad Sci USA 118. https://doi.org/10.1073/pnas.2103956118.
[10] Cotte, Y., Toy, F., Jourdain, P., Pavillon, N., Boss, D., Magistretti, P., et al., 2013. Marker-free phase nanoscopy. Nat Photonics 7, 113–117. https://doi.org/10.1038/nphoton.2012.329.
[11] Ding, J., Guan, Y., Cong, Y., Chen, L., Li, Y.F., Zhang, Lijuan, et al., 2020. Single-particle analysis for structure and iron chemistry of atmospheric particulate matter. Anal Chem 92, 975–982. https://doi.org/10.1021/acs.analchem.9b03913.
[12] Foroozandeh, P., Aziz, A.A., 2018. Insight into cellular uptake and intracellular trafficking of nanoparticles. Nanoscale Res Lett 13. https://doi.org/10.1186/s11671-018-2728-6.
[13] Fuzzi, S., Baltensperger, U., Carslaw, K., Decesari, S., Denier Van Der Gon, H., Facchini, M.C., et al., 2015. Particulate matter, air quality and climate: lessons learned and future needs. Atmos Chem Phys 15, 8217–8299. https://doi.org/10.5194/acp-15-8217-2015.
[14] Hadei, M., Naddafi, K., 2020. Cardiovascular effects of airborne particulate matter: a review of rodent model studies. Chemosphere 242. https://doi.org/10.1016/j.chemosphere.2019.125204.
[15] Huang, X., Zhou, Z., Liu, X., Li, J., Zhang, L., 2020. PM2.5 exposure induced renal injury via the activation of the autophagic pathway in the rat and HK-2 cell. Environ Sci Eur 32. https://doi.org/10.1186/s12302-020-00378-7.
[16] Huff, R.D., Carlsten, C., Hirota, J.A., 2019. An update on immunologic mechanisms in the respiratory mucosa in response to air pollutants. J Allergy Clin Immunol 143, 1989–2001. https://doi.org/10.1016/j.jaci.2019.04.012.
[17] Kallepitis, C., Bergholt, M.S., Mazo, M.M., Leonardo, V., Skaalure, S.C., Maynard, S.A., et al., 2017. Quantitative volumetric Raman imaging of three dimensional cell cultures. Nat Commun 8. https://doi.org/10.1038/ncomms14843.
[18] Kelly, F.J., Fussell, J.C., 2012. Size, source and chemical composition as determinants of toxicity attributable to ambient particulate matter. Atmos Environ 60, 504–526. https://doi.org/10.1016/j.atmosenv.2012.06.039.
[19] Kim, D., Oh, N., Kim, K., Lee, S.Y., Pack, C.G., Park, J.H., et al., 2018. Label-free high-resolution 3-D imaging of gold nanoparticles inside live cells using optical diffraction tomography. Methods 136, 160–167. https://doi.org/10.1016/j.ymeth.2017.07.008.
[20] Kim, K., Park, Y., 2017. Tomographic active optical trapping of arbitrarily shaped objects by exploiting 3D refractive index maps. Nat Commun 8, 1–8 fhttps://doi.org/10.1038/ncomms15340.
[21] Kim, K., Yoon, J., Park, Y., 2015. Optical diffraction tomography for simultaneous 3D visualization and tracking of optically trapped particles. In: Proceedings of the Asia communications and photonics conference 2015. Washington, D.C.: OSA. p. AM1I.4. Available from: https://doi.org/10.1364/ACPC.2015.AM1I.4.
[22] Kim, K., Lee, S., Yoon, J., Heo, J., Choi, C., Park, Y., 2016. Three-dimensional label-free imaging and quantification of lipid droplets in live hepatocytes. Sci Rep 6, 1–8. https://doi.org/10.1038/srep36815.
[23] Kim, S.W., Khang, D., 2015. Multiple cues on the physiochemical, mesenchymal, and intracellular trafficking interactions with nanocarriers to maximize tumor target efficiency. Int J Nanomed 10, 3989–4008. https://doi.org/10.2147/IJN.S83951.
[24] Kim, T.I., Kwon, B., Yoon, J., Park, I.J., Bang, G.S., Park, Y.K., et al., 2017. Antibacterial activities of graphene oxide-molybdenum disulfide nanocomposite films. ACS Appl Mater Interfaces 9, 7908–7917. https://doi.org/10.1021/acsami.6b12464.
[25] Li, C.H., Tsai, M.L., Chiou, H.Y., Lin, Y.C., Liao, W.T., Hung, C.H., 2022. Role of macrophages in air pollution exposure related asthma. Int J Mol Sci 23, 1–18. https://doi.org/10.3390/ijms232012337.
[26] Li, D., Li, Y., Li, G., Zhang, Y., Li, J., Chen, H., 2019. Fluorescent reconstitution on deposition of PM 2.5 in lung and extrapulmonary organs. Proc. Natl. Acad. Sci. USA 116, 2488–2493. https://doi.org/10.1073/pnas.1818134116.
[27] Li, N., Sioutas, C., Cho, A., Schmitz, D., Misra, C., Sempf, J., et al., 2003. Ultrafine particulate pollutants induce oxidative stress and mitochondrial damage. Environ Health Perspect 111, 455–460. https://doi.org/10.1289/ehp.6000.
[28] Liu, X., Ma, J., Ji, R., Wang, S., Zhang, Q., Zhang, C., et al., 2021. Biochar fine particles enhance uptake of benzo(a)pyrene to macrophages and epithelial cells via different mechanisms. Environ Sci Technol Lett 8, 218–223. https://doi.org/10.1021/acs.estlett.0c00900.

[29] Meng, J., Martin, R.V., Li, C., Van Donkelaar, A., Tzompa-Sosa, Z.A., Yue, X., et al., 2019. Source contributions to ambient fine particulate matter for Canada. Environ Sci Technol 53, 10269–10278. https://doi.org/10.1021/acs.est.9b02461.

[30] Mitchell, M.J., Billingsley, M.M., Haley, R.M., Wechsler, M.E., Peppas, N.A., Langer, R., 2021. Engineering precision nanoparticles for drug delivery. Nat Rev Drug Discov 20, 101–124. https://doi.org/10.1038/s41573-020-0090-8.

[31] Nääv, Å., Erlandsson, L., Isaxon, C., Åsander Frostner, E., Ehinger, J., Sporre, M.K., et al., 2020. Urban PM2.5 induces cellular toxicity, hormone dysregulation, oxidative damage, inflammation, and mitochondrial interference in the HRT8 trophoblast cell line. Front Endocrinol (Lausanne) 11, 1–11. https://doi.org/10.3389/fendo.2020.00075.

[32] Okada, T., Iwayama, T., Murakami, S., Torimura, M., Ogura, T., 2021. Nanoscale observation of PM2.5 incorporated into mammalian cells using scanning electron-assisted dielectric microscope. Sci Rep 11, 1–12. https://doi.org/10.1038/s41598-020-80546-0.

[33] Park, S., Ahn, J.W., Jo, Y., Kang, H.Y., Kim, H.J., Cheon, Y., et al., 2020. Label-free tomographic imaging of lipid droplets in foam cells for machine-learning-Assisted therapeutic evaluation of targeted nanodrugs. ACS Nano 14, 1856–1865. https://doi.org/10.1021/acsnano.9b07993.

[34] Park, S.-H., Yoon, S.-J., Choi, S., Jung, J., Park, J.-Y., Park, Y.-H., et al., 2022. Particulate matter promotes cancer metastasis through increased HBEGF expression in macrophages. Exp Mol Med. https://doi.org/10.1038/s12276-022-00886-x.

[35] Quezada-Maldonado, E.M., Sánchez-Pérez, Y., Chirino, Y.I., García-Cuellar, C.M., 2021. Airborne particulate matter induces oxidative damage, DNA adduct formation and alterations in DNA repair pathways. Environ Pollut 287. https://doi.org/10.1016/j.envpol.2021.117313.

[36] Roshanzadeh, A., Park, S., Ganjbakhsh, S.E., Park, J., Lee, D.H., Lee, S., et al., 2020. Surface charge-dependent cytotoxicity of plastic nanoparticles in alveolar Cells under cyclic stretches. Nano Lett 20, 7168–7176. https://doi.org/10.1021/acs.nanolett.0c02463.

[37] Schneider, C.A., Rasband, W.S., Eliceiri, K.W., 2012. NIH image to ImageJ: 25 years of image analysis. Nat Methods 9, 671–675. https://doi.org/10.1038/nmeth.2089.

[38] Schraufnagel, D.E., 2020. The health effects of ultrafine particles. Exp Mol Med 52, 311–317. https://doi.org/10.1038/s12276-020-0403-3.

[39] Shi, Y., Ji, Y., Sun, H., Hui, F., Hu, J., Wu, Y., et al., 2015. Nanoscale characterization of PM 2.5 airborne pollutants reveals high adhesiveness and aggregation capability of soot particles. Sci Rep 5, 1–10. https://doi.org/10.1038/srep11232.

[40] Sousa De Almeida, M., Susnik, E., Drasler, B., Taladriz-Blanco, P., Petri-Fink, A., Rothen-Rutishauser, B., 2021. Understanding nanoparticle endocytosis to improve targeting strategies in nanomedicine. Chem Soc Rev 50, 5397–5434. https://doi.org/10.1039/d0cs01127d.

[41] Sung, Y., Choi, W., Fang-Yen, C., Badizadegan, K., Dasari, R.R., Feld, M.S., 2009. Optical diffraction tomography for high resolution live cell imaging. Opt InfoBase Conf Pap 17. p. 1977–9. https://doi.org/10.1364/oe.17.000266.

[42] Tan, G., Li, J., Yang, Q., Wu, A., Qu, D.Y., Wang, Y., et al., 2018. Air pollutant particulate matter 2.5 induces dry eye syndrome in mice. Sci Rep 8, 1–13. https://doi.org/10.1038/s41598-018-36181-x.

[43] Touret, N., Paroutis, P., Grinstein, S., 2005. The nature of the phagosomal membrane: endoplasmic reticulum versus plasmalemma. J Leukoc Biol 77, 878–885. https://doi.org/10.1189/jlb.1104630.

[44] Touret, N., Paroutis, P., Terebiznik, M., Harrison, R.E., Trombetta, S., Pypaert, M., et al., 2005. Quantitative and dynamic assessment of the contribution of the ER to phagosome formation. Cell 123, 157–170. https://doi.org/10.1016/j.cell.2005.08.018.

[45] Wang, W.-X., 2022. Bioimaging of metals in environmental toxicological studies: linking localization and functionality. Crit Rev Environ Sci Technol 52, 3384–3414. https://doi.org/10.1080/10643389.2021.1934368.

[46] Wolf, I., Vetter, M., Wegner, I., Böttger, T., Nolden, M., Schöbinger, M., et al., 2005. The medical imaging interaction toolkit. Med Image Anal 9, 594–604. https://doi.org/10.1016/j.media.2005.04.005.

[47] Wolf I, Vetter M, Wegner I, Nolden M, Bottger T, Hastenteufel M, et al. , 2004. The medical imaging interaction toolkit (MITK): a toolkit facilitating the creation of interactive software by extending VTK and ITK. In: Galloway, Jr., R.L. (Ed.), Medical Imaging 2004: Visualization, Image-Guided Procedures, and Display. p. 16. Available from: https://doi.org/10.1117/12.535112.

[48] Wu, W., Jin, Y., Carlsten, C., 2018. Inflammatory health effects of indoor and outdoor particulate matter. J Allergy Clin Immunol 141, 833–844. https://doi.org/10.1016/j.jaci.2017.12.981.

[49] Xie, W., You, J., Zhi, C., Li, L., 2021. The toxicity of ambient fine particulate matter (PM2.5) to vascular endothelial cells. J Appl Toxicol 41, 713–723. https://doi.org/10.1002/jat.4138.

[50] Xing, Y.F., Xu, Y.H., Shi, M.H., Lian, Y.X., 2016. The impact of PM2.5 on the human respiratory system. J Thorac Dis 8, E69–E74. https://doi.org/10.3978/j.issn.2072-1439.2016.01.19.

[51] Yang, L., Li, C., Tang, X., 2020. The impact of PM2.5 on the host defense of respiratory system. Front Cell Dev Biol 8, 1–9. https://doi.org/10.3389/fcell.2020.00091.

[52] Zhang, R., Wang, G., Guo, S., Zamora, M.L., Ying, Q., Lin, Y., et al., 2015. Formation of urban fine particulate matter. Chem Rev 115, 3803–3855. https://doi.org/10.1021/acs.chemrev.5b00067.

[53] Zhou, W., Tian, D., He, J., Zhang, Li, Tang, X., Zhang, Lijun, et al., 2017. Exposure scenario: another important factor determining the toxic effects of PM2.5 and possible mechanisms involved. Environ Pollut 226, 412–425. https://doi.org/10.1016/j.envpol.2017.04.010.